Chinese Chemical Letters 36 (2025) 109914

Contents lists available at ScienceDirect

Chinese Chemical Letters

journal homepage: www.elsevier.com/locate/cclet

Curcumin-loaded ceria nanoenzymes for dual-action suppression of inflammation and alleviation of oxidative damage in the treatment of acute lung injury

Qi Huang[a,b,1], Jun Liao[c,d,e,1], Jingjing Li[a,b,1], Zhengyan Gu[b,d,1], Xinkang Zhang[b], Mingxue Sun[b], Wenqi Meng[b], Guanchao Mao[b], Zhipeng Pei[b], Shanshan Zhang[b], Songling Li[b], Chuan Zhang[e], Yunqin Wang[b], Jihao Liu[b], Tingbin Shu[b], Min Tao[b], Ying Lu[d,*], Kai Xiao[b,f,*], Qingqiang Xu[b,g,*], Jincai Lu[a,*]

[a] School of Traditional Chinese Materia Medica, Shenyang Pharmaceutical University, Shenyang 110016, China
[b] Lab of Toxicology and Pharmacology, Faculty of Naval Medicine, Naval Medical University, Shanghai 200433, China
[c] School of Basic Medical Sciences, Peking University, Beijing 100191, China
[d] Department of Pharmaceutical Sciences, School of Pharmacy, Naval Medical University, Shanghai 200433, China
[e] School of Medicine, Shanghai University, Shanghai 200444, China
[f] Marine Biomedical Science and Technology Innovation Platform of Lingang Special Area, Shanghai 201306, China
[g] Basic Medical Center for Pulmonary Disease, Naval Medical University, Shanghai 200433, China

ARTICLE INFO

Article history:
Received 26 February 2024
Revised 15 April 2024
Accepted 21 April 2024
Available online 22 April 2024

Keywords:
Ceria nanoenzymes
Curcumin
Acute lung injury
Oxidative damage
Inflammation
Nano delivery systems

ABSTRACT

Acute lung injury (ALI) is a critical respiratory disorder with a high mortality rate and is caused by several factors. Addressing oxidative stress and inflammation is a pivotal strategy for ALI treatment. In this study, we introduced a novel nanotherapeutic approach involving a curcumin-loaded ceria nanoenzyme delivery system tailored to counteract the multifaceted aspects of ALI. This system leverages the individual and combined effects of the components to provide a comprehensive therapeutic solution. The dual-action capability of this nanosystem was manifested by mitigating mitochondrial oxidative stress in lung epithelial cells and inhibiting the transient receptor potential melanosome-associated protein 2 (TRPM2)-NOD-like receptor thermal protein domain associated protein 3 (NLRP3) signaling pathway, offering a highly effective therapeutic approach to ALI. Our findings reveal the underlying mechanisms of this innovative nanodelivery system, showcasing its potential as a versatile strategy for ALI treatment and encouraging further exploration of nanoenzyme-based therapies for ALI.

Acute lung injury (ALI) is a severe pulmonary condition that poses significant clinical challenges owing to its complex pathophysiology characterized by intense inflammation and oxidative stress within lung tissues [1–4]. This condition, which can escalate to acute respiratory distress syndrome (ARDS) without prompt and effective intervention, requires innovative therapeutic strategies capable of addressing both the inflammatory cascade and resultant oxidative damage to pulmonary cells [5]. Despite existing treatments, such as pharmacological interventions and supportive care, the high morbidity and mortality rates associated with ALI/ARDS underscore the urgent need for more effective therapeutic approaches [6–8].

To meet this clinical need, the development of nanoenzymes that act as both drugs and carriers offers a promising avenue for the treatment of a wide range of diseases [9–15]. Cerium oxide nanoenzymes (CeO_2-NZs) are recognized for their unique catalytic properties that mimic natural enzymes such as superoxide dismutase (SOD) and catalase [16]. These nanoenzymes can modulate reactive oxygen species (ROS) levels, thereby reducing oxidative stress and inflammation in pulmonary tissues [17–20]. The high stability, physiological compatibility, and efficient ROS-scavenging capacity of CeO_2-NZs facilitate their application in biomedicine, making them ideal candidates for addressing the oxidative components of ALI [21–23]. Considering the complexity of ALI pathology, the therapeutic potential of CeO_2-NZs is greatly enhanced when combined with bioactive compounds with anti-inflammatory

* Corresponding authors.
E-mail addresses: acuace@163.com (Y. Lu), kaixiaocn@163.com (K. Xiao), xuqingqiang1027@126.com (Q. Xu), jincailu@syphu.edu.cn (J. Lu).
[1] These authors contributed equally to this work.

https://doi.org/10.1016/j.cclet.2024.109914
1001-8417/

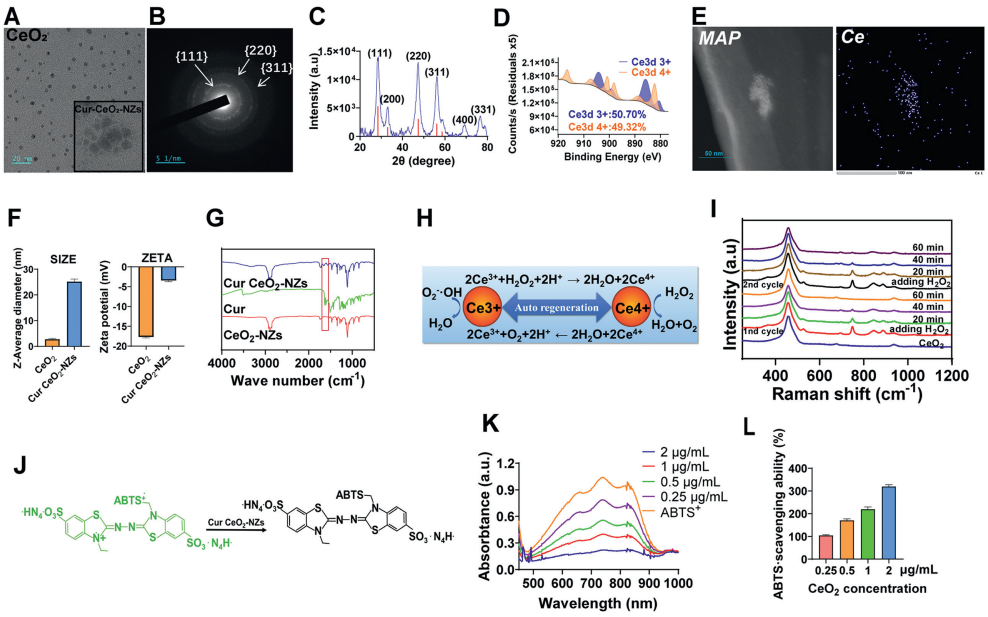

Fig. 1. Synthesis and characterization of Cur CeO_2-NZs. (A) High-resolution transmission electron micrographs of CeO_2 and Cur CeO_2-NZs. Scale bar: 20 nm. (B) Selected area electron diffraction. (C) The cubic fluorite structure of CeO_2. (D) XPS analysis of Ce 3d showing the binding energy (BE) levels of Ce(III) and Ce(IV). (E) High-angle annular dark-field scanning transmission images and energy dispersive spectrometer (EDS) mapping of Cur CeO_2-NZs. Scale bar: 50 nm. (F) Particle sizes and zeta potentials of CeO_2 and Cur CeO_2-NZs. (G) Infrared spectra of Cur CeO_2-NZs, Cur, and CeO_2-NZs. (H) A schematic diagram of the renewable cycle of CeO_2 for ROS scavenging. (I) Raman spectra of CeO_2 at different time points after reaction with H_2O_2. (J) A schematic illustration of the $ABTS^{+\bullet}$ radical scavenging process. (K) Ultraviolet–visible spectroscopy (UV–vis) absorption spectra and quantitative results. (L) For CeO_2 and $ABTS^{+\bullet}$ after incubation with different concentrations. All data are presented as the mean ± SD ($n = 3$).

properties [24]. Curcumin (Cur) is a polyphenolic compound extracted from turmeric and has been extensively studied for its anti-inflammatory and antioxidant properties [25–27]. Despite its promising therapeutic effects, the clinical application of Cur in ALI is severely limited because of its poor solubility, low stability, rapid metabolism, and low absorption, resulting in greatly reduced bioavailability. To address these limitations, we aimed to develop a novel nano-delivery system that synergistically combines the advantages of CeO_2-NZs with the therapeutic benefits of Cur. By encapsulating Cur within a nanoenzymatic framework of ceria nanoenzymes, Cur-loaded CeO_2-NZs (Cur CeO_2-NZs) were produced. Additionally, we attempted to enhance the solubility, stability, and cellular uptake of Cur to overcome its inherent pharmacokinetic limitations. This innovative approach not only enhances the antioxidant and anti-inflammatory efficacy of Cur but also leverages the ROS-scavenging capabilities of CeO_2-NZs, offering a dual-action therapeutic strategy for the effective management of ALI (Scheme S1 in Supporting information).

CeO_2-NZs were synthesized *via* a complex process, which is shown in Scheme S1. Initially, hydrophobic ceria was synthesized *via* pyrolysis. Subsequent examination using transmission electron microscopy (TEM) illustrated a uniform dispersion of CeO_2 nanoparticles in water, manifesting as ultrasmall nanodots with a mean diameter (Fig. 1A). The crystal structure was confirmed through selected-area electron diffraction (SAED) (Fig. 1B) and X-ray diffraction (XRD) analyses (Fig. 1C), both of which confirmed the cubic fluorite structure of the nanoparticles. Further characterization through X-ray photoelectron spectroscopy (XPS) (Fig. 1D) verified the synthesis of divalent ceria NZs, with spectra revealing Ce(III) oxide peaks at specific energy values alongside Ce(IV) oxide peaks, indicating a composition of 50.70% Ce(III) oxide and 49.32% Ce(IV) oxide. This composition underscores the significant role of Ce(IV) oxide in the cyclic scavenging of ROS. To enhance biocompatibility, CeO_2 nanoparticles were functionalized using 1,2-distearoyl-*sn*-glycero-3-phosphoethanolamine-*N*-[methoxy(polyethylene glycol)-2000] (DSPE-PEG_{2000}). The modification process employed a thin-film dispersion method, followed by purification through dialysis. Concurrently with CeO_2-NZs synthesis, Cur was incorporated, resulting in the formation of Cur CeO_2-NZs through van der Waals forces and organic macromolecule adsorption (Scheme S1 and Fig. S1 in Supporting information). TEM analysis of the Cur CeO_2-NZs (Fig. 1A) confirmed their uniform dispersion in water, with an average size of 25 nm. High-angle annular dark-field scanning transmission electron microscopy (HAADF-STEM) (Fig. 1E) demonstrated successful surface modification, which was further evidenced by the coherent overlay of Ce signals with the NZs. Physicochemical properties, including particle size and surface charge, were assessed using laser particle sizing and zeta potential measurements (Fig. 1F), which revealed notable changes after Cur and DSPE-PEG_{2000} modification. Infrared spectroscopy analysis provided additional confirmation of Cur loading onto CeO_2-NZs, highlighted by the appearance of characteristic Cur peaks in the Cur CeO_2-NZs spectrum (Fig. 1G). Quantitative analysis of Cur loading was performed using the external standard method, establishing a drug-loading efficiency of 4.8% and an encapsulation rate of 73.7% (Fig. S2 in Supporting information). *In vitro* release studies in phosphate buffered saline (PBS) showed an initial rapid release of 23% of the loaded Cur within the first 2 h, followed by a gradual release of 54.67% within 48 h (Fig. S3 in Supporting information). In addition, the modified Cur CeO_2-NZs were found to have good particle size stability (Fig. S4 in Supporting information), indicating their suitability for biomedical applications.

Excessive ROS production induces mitochondrial dysfunction, which is a precursor of ALI development. The reversible oxidation state transitions of CeO_2 endow it with dynamic and recyclable ROS neutralization capabilities (Fig. 1H). To elucidate CeO_2 catalytic efficacy and regeneration during its interaction with hydrogen peroxide (H_2O_2), *in situ* Raman spectroscopy was performed using a 532-nm laser excitation source. Remarkably, the Raman spectral alterations observed in the subsequent cycles upon the reintroduction of H_2O_2 mirrored the initial observations, underscoring the exceptional reusability of CeO_2 as an antioxidant (Fig.

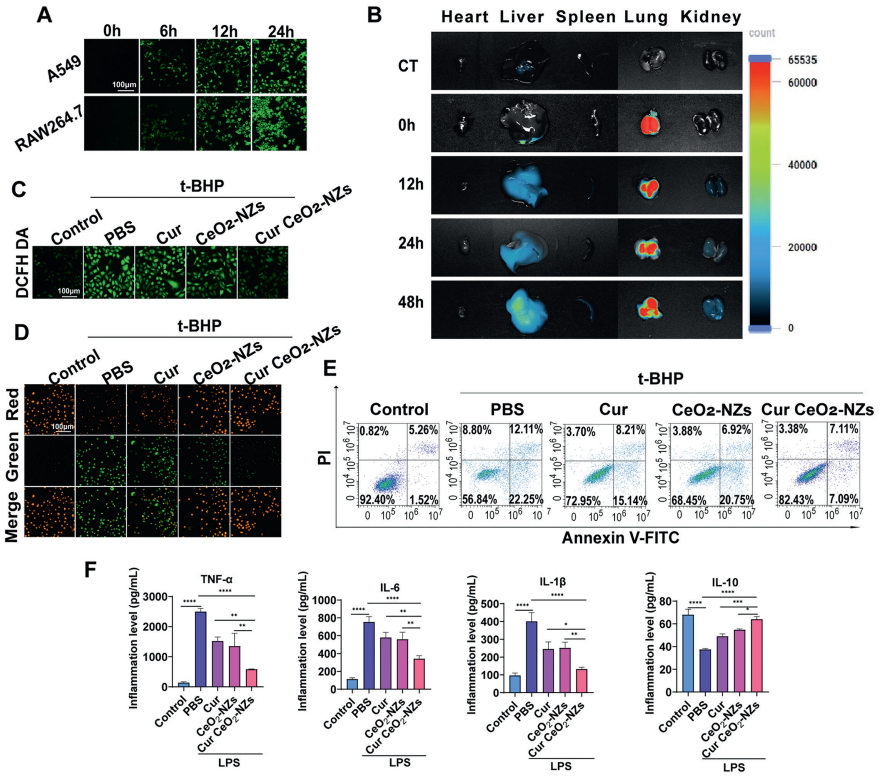

Fig. 2. Uptake of Cur CeO_2-NZs and their anti-inflammatory and antioxidant effects in cells. (A) Uptake of FITC-labeled Cur CeO_2-NZs by A549 and RAW264.7 cells. (B) Fluorescence imaging of organs after tracheal nebulization administration of nanoparticles loaded with Cy5.5 dye in mice. (C) Representative images of intracellular ROS levels in A549 cells. (D) Representative images of the mitochondrial membrane potential of A549 cells. (E) Annexin V-fluorescein isothiocyanate (FITC)/propidium iodide (PI) double staining evaluation of the reversal of *t*-BHP-induced apoptosis. (F) Levels of inflammatory factors in the supernatant of RAW264.7 cells. All data are presented as the mean ± SD ($n = 3$). $^{*}P < 0.05$, $^{**}P < 0.01$, $^{***}P < 0.001$, $^{****}P < 0.0001$. Scale bar: 100 μm.

1I). Furthermore, the antioxidant potential of CeO_2 was quantified using 2,2′-azo-3-ethylbenzothiazole-6-sulfonate (ABTS) assay across varying concentrations and durations (Fig. 1J). ABTS+ cation radicals, which are characterized by their blue-green coloration, are decolorized upon reduction with antioxidants. Dose-dependent decolorization, as evidenced by the diminished absorption peak at 734 nm with increasing CeO_2 concentration, indicated a pronounced inhibitory effect on ABTS radical generation (Fig. 1K). At a concentration of 2 μg/mL, CeO_2 demonstrated significant ABTS radical scavenging activity, highlighting its potential as an effective antioxidant and ROS scavenger (Fig. 1L). The above results show that CeO_2 is able to scavenge free radicals cyclically, which makes CeO_2 characterized by long-lasting and high efficiency. Compared with traditional antioxidants, CeO_2 can maintain a higher antioxidant effect after multiple uses. CeO_2 can efficiently scavenge free radicals and other harmful oxidizing substances. These properties render CeO_2 as a promising candidate for mitigating oxidative stress-induced damage, particularly in conditions such as ALI.

Following meticulous characterization of Cur CeO_2-NZs, a comprehensive set of cellular and animal experiments was conducted to evaluate their biocompatibility, therapeutic efficacy, and safety profiles. The cellular uptake of these Cur CeO_2-NZs was first assessed using fluorescence microscopy after treating A549 lung epithelial cells and RAW264.7 macrophages with FITC-labeled Cur CeO_2-NZs at various culturing intervals. A time-dependent increase in cellular uptake was observed, affirming efficient internalization of the Cur CeO_2-NZs and potential for intracellular therapeutic action (Fig. 2A and Fig. S5 in Supporting information). To extend these observations *in vivo*, mice were administered Cy5.5-labeled Cur CeO_2-NZs *via* tracheal nebulization. All animal procedures performed in this study were in accordance with the ethical guidelines approved by the Animal Care and Use Committee of Naval Medical University (approval No. 20210310013). Subsequent organ harvesting and imaging demonstrated pronounced fluorescence in lung tissues immediately after administration, with detectable fluorescence persisting for up to 48 h. This indicates the sustained bioavailability and effectiveness of Cur CeO_2-NZs when administered through nebulization, showing prolonged engagement with the lung tissue (Fig. 2B and Fig. S6 in Supporting information). The biocompatibility of Cur CeO_2-NZs was further explored by evaluating their cytotoxicity in A549 cells at varying concentrations over a 24 h period using a cell counting kit-8 (CCK-8) assay. Results indicated negligible cytotoxicity, even at concentrations as high as 100 μg/mL, with cell viabilities exceeding 80%. Similar non-toxic profiles were observed in RAW264.7 cells, suggesting that Cur CeO_2-NZs do not interfere with cellular growth (Fig. S7 in Supporting information). Animal studies were conducted to assess the *in vivo* safety of Cur CeO_2-NZs administered *via* tracheal nebulization. Subsequent pathological analyses of vital organs at 48 h and 14 d post-administration revealed no abnormal histopathological changes, confirming the safety profile of Cur CeO_2-NZs (Figs. S8 and S9 in Supporting information). In the cell, the site of ROS generation is the mitochondria, and the nanoenzymes enter the cell; according to the nature of CeO_2, they can be targeted toward the mitochondria to scavenge ROS (Fig. S10 in Supporting information). The protective efficacy of the Cur CeO_2-NZs against oxidative stress was investigated using a *t*-BHP-induced oxidative damage model in A549 cells. The half maximal inhibitory concentration (IC_{50}) value of *t*-BHP was used as the concentration (Fig. S11 in Supporting information). Treatment with Cur CeO_2-NZs significantly mitigated intracellular ROS levels, outperforming Cur and CeO_2-NZs alone, indicating their superior antioxidant properties (Fig. 2C and Fig.

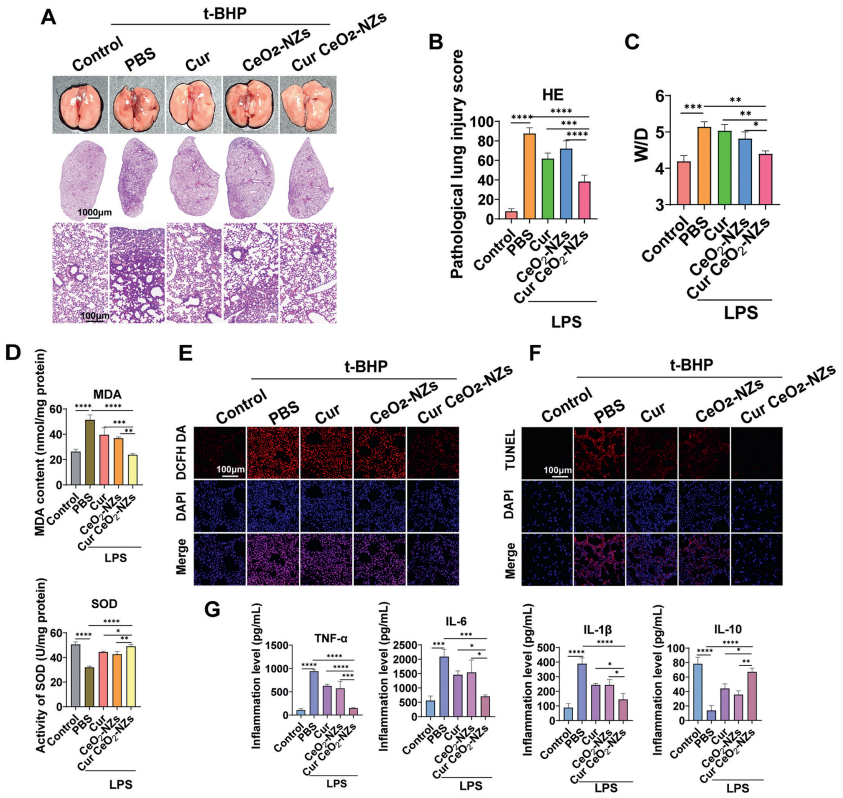

Fig. 3. Cur CeO_2-NZs provide protection against LPS-induced acute lung injury. (A) Hematoxylin and eosin staining of the lung tissues of mice. (B) Statistical graph of the scores of hematoxylin and eosin staining of mouse lung tissues. (C) Wet-to-dry weight ratio of lung tissues. (D) MDA and SOD contents in the lung tissue homogenates of mice. (E) DCFH-DA staining of mouse lung tissues. DAPI, 4′,6-diamidino-2-phenylindole. (F) TUNEL staining of mouse lung tissues. (G) Inflammatory factor levels in alveolar lavage fluid. All data are presented as the mean ± SD ($n = 3$). $^{*}P < 0.05$, $^{**}P < 0.01$, $^{***}P < 0.001$, $^{****}P < 0.0001$. Scale bar: 100 μm.

S12 in Supporting information). Additionally, Cur CeO_2-NZs effectively preserved the mitochondrial membrane potential under oxidative stress, demonstrating enhanced protective effects on mitochondrial integrity compared with those of the control treatments (Fig. 2D and Fig. S13 in Supporting information). Furthermore, Cur CeO_2-NZs significantly reduced *t*-BHP-induced apoptosis, demonstrating their potential to prevent cell death (Fig. 2E and Fig. S14 in Supporting information). In an *in vitro* inflammation model using lipopolysaccharides (LPS)-stimulated RAW264.7 cells, Cur CeO_2-NZs markedly downregulated pro-inflammatory cytokines (tumor necrosis factor-alpha (TNF-α), interleukin-6 (IL-6), IL-1β) and upregulated anti-inflammatory cytokines IL-10 compared with controls, highlighting their anti-inflammatory capabilities (Fig. 2F). Collectively, these findings suggest that Cur CeO_2-NZs not only exhibit promising biocompatibility and safety both *in vitro* and *in vivo* but also demonstrate significant protective effects against oxidative stress and inflammation, positioning them as potent therapeutic agents for lung epithelial protection and inflammation mitigation.

In a comprehensive study aimed at exploring the therapeutic potential of Cur CeO_2-NZs in ALI, an LPS-induced C57BL/6 mouse model was established (Fig. S15 in Supporting information). Histological assessment of lung sections using hematoxylin and eosin (HE) staining revealed significant structural damage in LPS-exposed mice, characterized by diffuse interstitial edema, reduced alveolar space, thickened alveolar walls, and extensive infiltration by inflammatory cells. This damage indicated a compromised pulmonary blood-air barrier, further highlighted by the presence of red blood cells within the alveoli. In this study, we used the lung injury score derived from the scoring system (Table S1 in Supporting information). Notably, treatment with Cur CeO_2-NZs profoundly ameliorated these pathological alterations, highlighting their superior therapeutic efficacy (Figs. 3A and B). Analysis of the body weights revealed a reversal of LPS-induced weight loss in mice, especially in those treated with Cur CeO_2-NZs, suggesting an enhanced recovery (Fig. S16 in Supporting information). Morphometric analysis of the lung tissue further supported the therapeutic benefits of Cur CeO_2-NZs, showing improved alveolar structural integrity, as evidenced by decreased alveolar septal thickness and increased alveolar count per high-power field, compared with the PBS group (Fig. S17 in Supporting information). We measured the wet-to-dry weight ratio (W/D) of lung tissue to assess pulmonary edema and found a significant reduction in the W/D ratio among treated mice, particularly with Cur CeO_2-NZs (Fig. 3C). Moreover, analysis of lung tissue homogenates indicated a notable decrease in malondialdehyde (MDA) levels and an increase in SOD activity in mice treated with Cur CeO_2-NZs, indicating reduced oxidative stress and enhanced antioxidative defense (Fig. 3D). Furthermore, 2′,7′-dichlorodihydrofluorescein diacetate (DCFH-DA) staining for quantifying ROS levels showed a significant reduction in ROS in the Cur CeO_2-NZs-treated group than in the PBS group, indicating effective ROS mitigation (Fig. 3E and Fig. S18 in Supporting information). Terminal deoxynucleotidyl transferase-mediated dUTP-biotin nick end labeling (TUNEL) staining revealed a decrease in LPS-induced apoptosis in pulmonary tissues following Cur CeO_2-NZs treatment, which was consistent with earlier cellular findings (Fig. 3F and Fig. S19 in Supporting information). Immunohistochemical analysis using 8-hydroxy-2′-deoxyguanosine (8-OHdG) highlighted reduced oxidative DNA damage following Cur CeO_2-NZs treatment (Fig. S20 in Supporting information). Lastly, analysis of bronchoalveolar lavage fluid (BALF) demonstrated that Cur CeO_2-NZs treatment significantly attenuated pro-inflammatory cy-

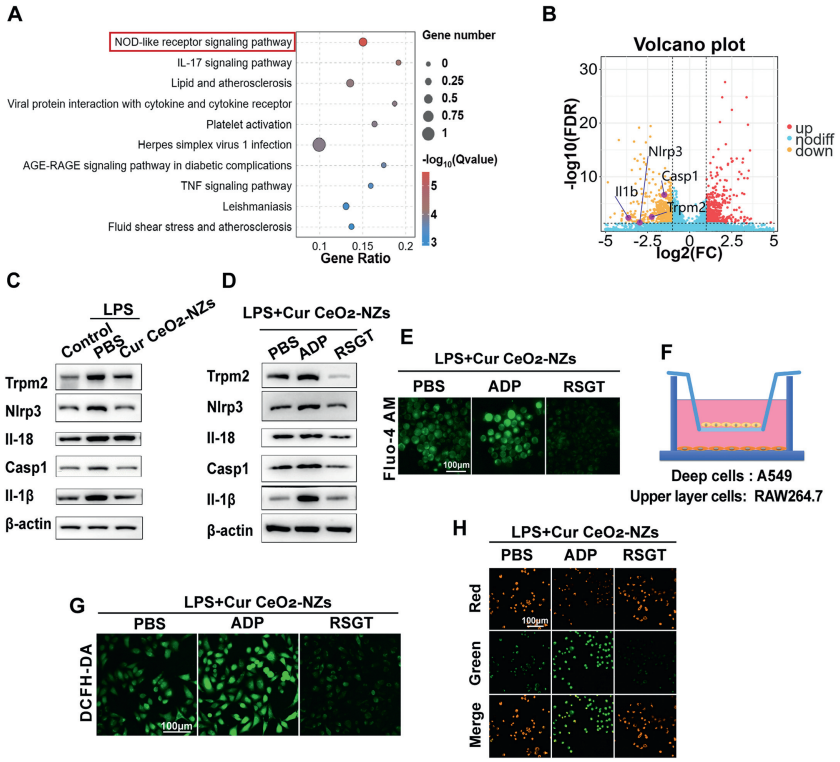

Fig. 4. RNA sequencing analysis of acute lung injury mouse tissues treated with Cur CeO_2-NZs and target validation. (A) Pathways of the top 10 significantly enriched differentially expressed genes (DEGs). (B) Volcano plots for all DEGs between the control and Cur CeO_2-NZs. The dots represent DEGs (FDR $\leq$ 0.001, at least two-fold differences). (C) Expression of key proteins. (D) Expression of key proteins in RAW264.7 cells following treatment with an agonist or inhibitor of TRPM2. (E) Calcium fluorescence of RAW264.7 cells following treatment with an agonist or inhibitor of TRPM2. (F) A schematic diagram showing the Transwell setup. (G) The effects of TRPM2 agonist or inhibitor on ROS fluorescence intensity in A549 cells. (H) JC-1 fluorescence plots of A549 cells treated with an agonist or inhibitor of TRPM2. All data are presented as the mean ± SD ($n = 3$). $^{*}P < 0.05$, $^{**}P < 0.01$, $^{***}P < 0.001$, $^{****}P < 0.0001$. Scale bar: 100 μm.

tokine levels (TNF-α, IL-6, IL-1β) and increased anti-inflammatory cytokine IL-10 levels, indicating an effective anti-inflammatory response and improved alveolar-capillary barrier function (Fig. 3G and Fig. S21 in Supporting information). Collectively, these findings delineate the multifaceted therapeutic efficacy of Cur CeO_2-NZs in mitigating oxidative stress, reducing inflammation, and promoting lung tissue recovery in ALI, demonstrating their potential as a novel treatment strategy.

To elucidate the therapeutic mechanisms of Cur CeO_2-NZs in ALI, we conducted a transcriptome sequencing analysis of lung tissue samples from mice before and after treatment with Cur CeO_2-NZs. Understanding the type, amount, and expression levels of RNA in the cell is crucial to reveal the function and regulatory mechanism of genes. Principal component analysis plots of the sequencing results confirmed good reproducibility of samples within groups, significant differences between samples between groups, and the usability of sequencing data (Fig. S22 in Supporting information). Kyoto encyclopedia of genes and genomes (KEGG) enrichment analysis revealed that the differentially expressed genes were significantly enriched in the nucleotide-binding oligomerization domain (NOD)-like receptor signaling pathway (Fig. 4A), a pathway closely associated with inflammation and oxidative damage, primarily involving the NOD-like receptor pyrin domain-containing 3 (NLRP3) inflammasome. The results of hierarchical clustering analysis revealed that the differential expression of these genes was more pronounced in the Cur CeO_2-NZs-treated group and that there were significant differences in the mRNA profiles obtained for the lung tissues of the Cur CeO_2-NZs- and LPS-treated mice with ALI (Fig. S23 in Supporting information). Based on the volcano plot analysis of the transcriptome data, we identified 22,183 genes in both the ALI and Cur CeO_2-NZs groups. Genes with a log2 (fold change) expression $\geq$ 1.0 and $\leq$ 1.0 were considered to be significantly up- and down-regulated, respectively (treatment *vs.* control) (Fig. 4B). Notably, genes with pronounced expression differences in the NOD-like receptor signaling pathway included those encoding the transient receptor potential melanosome-associated protein 2 (TRPM2), NLRP3, cysteinyl aspartate specific proteinase 1 (CASP1), and IL-1β proteins (Fig. S24 in Supporting information). The protein expression of these genes was validated using western blot analysis, and the findings were consistent with the transcriptome sequencing results (Fig. 4C).

Transient receptor potential (TRP) ion channels are a class of widely distributed channel proteins, and there is ample evidence to indicate that these channels play a key role in regulating intracellular Ca^{2+} concentrations [28]. As calcium ions are a major trigger for NLRP3 inflammasome activation [29]. In response to the activation of inflammasomes, CASP1 is cleaved, thereby indirectly promoting the synthesis and release of inflammatory factors such as IL-1β and IL-18. CASP1 also facilitates GSDMD synthesis, leading to cell pyroptosis [30–32]. We hypothesized that Cur CeO2-NZs regulate TRP levels by modulating the expression or activity of TRPM2, thereby influencing the NLRP3 inflammatory signaling pathway.

To establish whether the therapeutic effects of Cur CeO_2-NZs are mediated *via* modulation of the TRPM2-NLRP3 signaling pathway, we performed immunofluorescence staining of mouse lung tissues. The results showed that Cur CeO_2-NZs were able to reduce the expression of TRPM2 in lung tissues (Fig. S25 in Supporting information). Furthermore, we co-administered the TRPM2 protein activator adenosine 5′-diphosphoribose sodium (ADP) and the inhibitor rosiglitazone maleate (RSGT) with Cur CeO_2-NZs. Initially, we assessed the effects on inflammatory factors in RAW264.7 cells and found that the TRPM2 activator suppressed the inhibitory ef-

fects of Cur CeO_2-NZs on pro-inflammatory factors, thereby leading to enhanced inflammation. Conversely, the TRPM2 inhibitor synergistically enhanced the inhibitory effect of Cur CeO_2-NZs on the pro-inflammatory factors (Fig. S26 in Supporting information). Analysis of the effects on the protein components of the TRPM2-NLRP3 signaling pathway revealed that the TRPM2 activator disrupted the inhibitory effect of Cur CeO_2-NZs on this pathway, whereas the TRPM2 inhibitor synergistically enhanced this inhibitory effect (Fig. 4D). A Fluo-4AM calcium ion detection probe was used to monitor the intracellular calcium ion levels in RAW264.7 cells, which revealed a significant enhancement of calcium ion fluorescence in the activator group, whereas fluorescence was markedly reduced in the inhibitor group (Fig. 4E and Fig. S27 in Supporting information).

Based on these findings, we established an *in vitro* co-culture model using RAW264.7 and A549 cells to simulate the damaging effects of *in vivo* inflammation on pulmonary epithelial cells (Fig. 4F). After initial stimulation of RAW264.7 cells with LPS, followed by treatment with Cur CeO_2-NZs, we separately administered the TRPM2 protein activator and inhibitor to assess their effects on A549 cell ROS levels and mitochondrial damage. Treatment with Cur CeO_2-NZs inhibited the inflammation-induced generation of ROS and the decline in mitochondrial membrane potential in A549 cells. However, while the TRPM2 activator disrupted these effects, the TRPM2 inhibitor synergistically enhanced the inhibitory effects of Cur CeO_2-NZs against oxidative damage (Figs. 4G and H, Figs. S28 and S29 in Supporting information). These findings further confirmed that the therapeutic effects of Cur CeO_2-NZs were mediated *via* the inhibition of the TRPM2-NLRP3 signaling pathway.

Conclusively, we designed and synthesized a novel drug delivery system consisting of ceria nanoenzymes as carriers, which were loaded with the anti-inflammatory drug Cur to obtain Cur CeO_2-NZs. This innovative design offers several notable advantages, including enhanced biocompatibility, a low metabolic rate, high utilization, mitochondrial targeting, and cyclic scavenging of free radicals. Our results revealed that treatment with this system effectively regulated the mitochondrial membrane potential, restored mitochondrial function, reduced intracellular ROS generation, reduced inflammasome formation, regulated the release of inflammatory factors, and synergistically promoted anti-inflammatory and antioxidant effects. Therefore, we believe that this novel nanodrug delivery system has considerable therapeutic potential in the treatment of ALI.

Declaration of competing interest

The authors declare that they have no competing financial interests or personal relationships that could have influenced the work reported in this study.

CRediT authorship contribution statement

Qi Huang: Writing – review & editing, Writing – original draft, Investigation, Data curation. **Jun Liao:** Resources, Methodology, Conceptualization. **Jingjing Li:** Methodology, Conceptualization. **Zhengyan Gu:** Conceptualization. **Xinkang Zhang:** Visualization, Conceptualization. **Mingxue Sun:** Project administration. **Wenqi Meng:** Validation. **Guanchao Mao:** Validation. **Zhipeng Pei:** Visualization. **Shanshan Zhang:** Software, Conceptualization. **Songling Li:** Resources. **Chuan Zhang:** Supervision. **Yunqin Wang:** Visualization. **Jihao Liu:** Investigation. **Tingbin Shu:** Formal analysis. **Min Tao:** Resources, Conceptualization. **Ying Lu:** Writing – review & editing, Funding acquisition. **Kai Xiao:** Funding acquisition. **Qingqiang Xu:** Writing – original draft, Supervision, Funding acquisition. **Jincai Lu:** Supervision, Funding acquisition.

Acknowledgments

This work was funded by the National Natural Science Foundation of China (Nos. 82103885, 81871521, 82273672), Natural Science Foundation of Shanghai (Nos. 21ZR1477700, 20ZR1470300), the Shanghai Municipal Health Commission-Outstanding Youth Foundation of Public Health (No. GWV-10.2-YQ48), and SciTech Funding by CSPFTZ Lingang Special Area Marine Biomedical Innovation Platform.

Supplementary materials

Supplementary material associated with this article can be found, in the online version, at doi:10.1016/j.cclet.2024.109914.

References

[1] S.R. Leist, K.H. Dinnon, A. Schäfer, et al., Cell 183 (2020) 1070–1085.
[2] W. Zhong, X. Zhang, Y. Zeng, et al., Nano Res. 14 (2021) 2067–2089.
[3] Y. Wang, Q. Li, M. Deng, et al., Chin. Chem. Lett. 33 (2022) 324–327.
[4] H. Wu, F. Li, S. Wang, et al., Biomaterials 151 (2018) 66–77.
[5] C. Zhuang, M. Kang, M. Lee, J. Control. Release 360 (2023) 1–14.
[6] Y. Li, J. Liao, L. Xiong, et al., J. Control. Release 368 (2024) 607–622.
[7] C. Liu, J. Yao, J. Hu, et al., Mater. Horiz. 7 (2020) 3176–3186.
[8] Y. Meng, S. Han, J. Yin, J. Wu, ACS Appl. Mater. Interfaces 15 (2023) 41743–41754.
[9] C. Liu, W. Fan, W.X. Cheng, et al., Adv. Funct. Mater. 33 (2023) 2213856.
[10] J. Liao, Y. Li, L. Fan, et al., ACS Nano 18 (2024) 5510–5529.
[11] C. Liu, J. Xing, O.U. Akakuru, et al., Nano Lett. 19 (2019) 5674–5682.
[12] C. Liu, L. Luo, L. Zeng, et al., Small 14 (2018) 1801851.
[13] J. Liu, D. He, T. Hao, et al., Chin. Chem. Lett. 35 (2024) 109296.
[14] Z. Wu, H. Wang, S. Fang, C. Xu, Mol. Med. Rep. 18 (2018) 4163–4174.
[15] Y. Wang, H. Dong, H. Qu, et al., Nano Lett. 24 (2024) 2131–2141.
[16] F. Zeng, Y. Wu, X. Li, et al., Angew. Chem. Int. Ed. 57 (2018) 5808–5812.
[17] J. Liao, Y. Li, Y. Luo, et al., Mol. Pharm. 19 (2022) 3026–3041.
[18] J. Liao, L. Fan, Y. Li, et al., J. Control. Release 358 (2023) 439–464.
[19] C. Xie, J. Liao, N. Zhang, et al., Chin. Chem. Lett. 35 (2024) 109149.
[20] R. Yuan, Y. Li, S. Han, et al., ACS Cent. Sci. 8 (2021) 10–21.
[21] H. He, L. Du, H. Xue, et al., Small Methods 7 (2023) 2300230.
[22] L. Sun, Y. Liu, X. Liu, et al., Adv. Sci. 9 (2022) 2104051.
[23] C. Liu, L. Xi, Y. Liu, et al., ACS Nano 17 (2023) 11626–11644.
[24] A. Unlu, E. Nayir, M. Dogukan Kalenderoglu, et al., J. BUON 21 (2016) 1050–1060.
[25] J. Gao, Z. Weng, Z. Zhang, et al., Adv. Healthc. Mater. 13 (2024) 2303095.
[26] A. Farazin, M. Mohammadimehr, A.H. Ghasemi, H. Naeimi, RSC Adv. 11 (2021) 32775–32791.
[27] H. Wei, D. Jiang, B. Yu, et al., Bioact. Mater. 19 (2023) 282–291.
[28] N.J. Himmel, D.N. Cox, Proc. Biol. Soc. 287 (2020) 20201309.
[29] E. Jäger, S. Murthy, C. Schmidt, et al., Nat. Commun. 11 (2020) 4243.
[30] K. Wang, Q. Sun, X. Zhong, et al., Cell 180 (2020) 941–955.
[31] L. Meng, X. Zhao, H. Zhang, Med. Sci. Monit. 25 (2019) 827–835.
[32] F.J. Bock, S.W.G. Tait, Nat. Rev. Mol. Cell Biol. 21 (2020) 85–100.